UCLA
COMPUTATIONAL AND APPLIED MATHEMATICS

Numerical Computation of Self-Similar Solutions for Mean Curvature Flow

David L. Chopp

June 1993

CAM Report 93-17

Department of Mathematics
University of California, Los Angeles
Los Angeles, CA. 90024-1555

Numerical Computation of Self-Similar Solutions for Mean Curvature Flow

David L. Chopp

June 25, 1993

1 Introduction

Self-similar solutions of motion by mean curvature are an important component in the current research of the singularities in that motion. There appears to be a link between singularities in motion by mean curvature and self-similar shapes. For curves in R^2, Grayson [7] has proven that curves under motion by curvature shrink to round points. Alternatively, this shows that every closed embedded curve in R^2 deforms towards a self-similar solution as it approaches singularity, and that a circle is the only such self-similar solution. Therefore, Grayson's result effectively shows the connection between self-similar solutions and singularity.

For two-dimensional manifolds in R^3, the problem is much more difficult and not as well understood. However, two results by Huisken indicate that self-similar solutions and singularities are connected in this higher dimension as well. The first result, see [9], shows that convex manifolds shrink to spheres under motion by mean curvature. In [8], Grayson was able to prove that the convexity condition is necessary. In a recent paper by Angenent [1], he first proves the existence of a self-similar torus, then uses that torus to give an alternative proof that the convexity condition is necessary. This demonstrates the utility of self-similar solutions towards studying singularities. The best result showing the link between self-similarity and singularity is by Huisken [10] where he proves that if the curvature at a singularity is bounded by $c(T-t)^{-1/2}$, where t is time, T is the time of singularity and c is a constant, then the surface evolves towards a self-similar surface at the point of singularity.

At present, very few examples of two-dimensional embedded self-similar solutions for motion by mean curvature are proven to exist, all of them being surfaces of revolution. In this paper, we design a numerical algorithm to compute approximations to other self-similar solutions. We will give strong numerical evidence that these are good approximations to self-similar solutions.

In the next section we describe the algorithm including the modified form of motion by mean curvature differential equation. In the following section, we

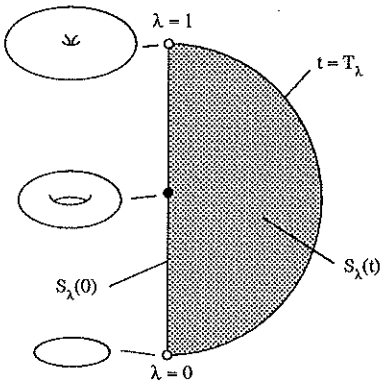

Figure 1: Diagram of $U \subset M$

discuss the reliability of the results in several different ways. In the final section we show a collection of approximate self-similar solutions for motion by mean curvature.

2 The Algorithm

The algorithm we use is based upon the level set method for propagating interfaces introduced by Osher and Sethian [11]. The theoretical aspects of this method were studied by Evans and Spruck [3, 4]. For further theoretical work, see also [2, ?, 5, 6]. It will be helpful to give a brief overview of the level set method as it applies here.

The idea behind the level set method is to represent a given two-dimensional manifold as a level set of a function $\phi : R^3 \times R \rightarrow R$. Thus, the set

$$S_\alpha(t) = \{x \in R^3 : \phi(x,t) = \alpha\}$$

represents the evolution of the α-level set in time t. Motion by mean curvature can now be expressed in terms of ϕ by

$$\phi_t(x,t) = \kappa_\phi(x,t)||\nabla\phi(x,t)||$$

where $\kappa_\phi(x,t)$ is the mean curvature of the $\phi(x,t)$ level set. Notice that this equation does not depend upon the level set value, each level set surface moves according to its own mean curvature. In this way, this equation evolves a continuous family of initial surfaces by mean curvature simultaneously. It is this property which is at the heart of our algorithm.

We introduce the self-similar algorithm by studying the case of finding a self-similar torus. let $\mathcal{M}$ be the space of all compact two-dimensional differentiable

manifolds embedded in R^3. For any two manifolds A, $B \in \mathcal{M}$, define the equivalence relation $A \sim B$ if B can be obtained from A by rigid body motion, rotation, and uniform stretching. Now let $M = \mathcal{M}/\sim$.

Let $C = \{x = (x_1, x_2, x_3) \in R^3 : x_1^2 + x_2^2 = 1, x_3 = 0\}$ and define $S_\lambda(0) = \{x \in R^3 : \text{dist}(x, C) = \lambda\}$. Thus, $S_\lambda(0)$ is a one-dimensional subspace of M parameterized by $\lambda \in (0, 1)$. For each λ, let $S_\lambda(t)$ be the result of moving $S_\lambda(0)$ by mean curvature to time t, and define T_λ as the time to singularity for the initial surface $S_\lambda(0)$. We now have a subset $U = \{S_\lambda(t) : \lambda \in (0, 1), t \in [0, T_\lambda)\} \subset M$. A diagram of U is shown in Figure 1.

Next, we define a ratio function $\rho : U \to R$, $\rho(A) = m_2/m_1$, where m_2 is the maximum height of the torus in the z direction and m_1 is the innermost radius of the torus as shown in Figure 2. Thus, $\rho(S_\lambda(0)) \to +\infty$ as $\lambda \to 1^-$

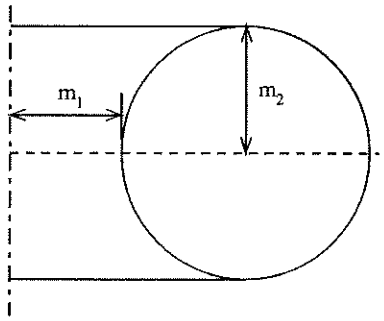

Figure 2: Measurements of a torus for computing ρ.

and $\rho(S_\lambda(0)) \to 0^+$ as $\lambda \to 0^+$. We rescale U in terms of ρ and t so that U is contained in the shaded region in Figure 3.

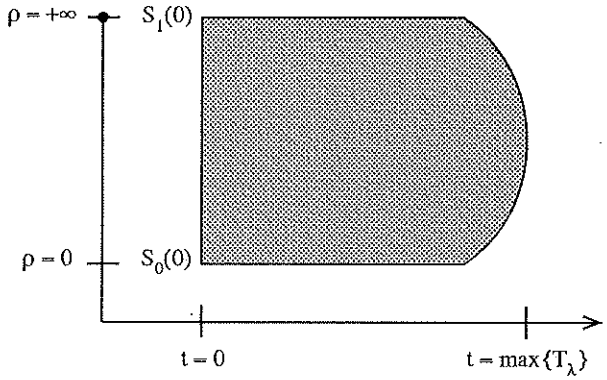

Figure 3: Rescaled diagram of U.

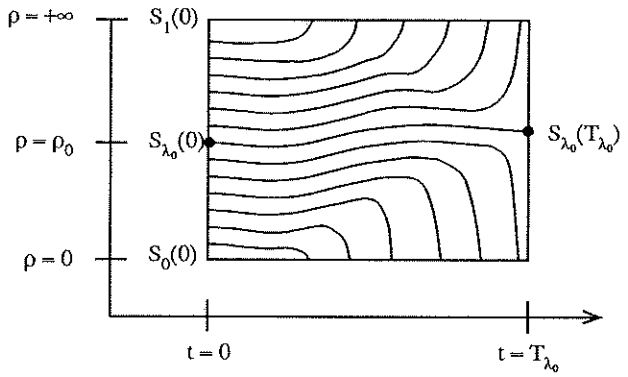

Figure 4: Plot of trajectories for $S_\lambda(t)$

If we turn our attention now to the trajectories $S_\lambda(t)$, $t \in [0, T_\lambda)$, we see that there is a value λ_0 such that if $\lambda > \lambda_0$, then $\rho(S_\lambda(t)) \to +\infty$, $\frac{d}{dt}\rho(S_\lambda(t)) > 0$, as $t \to T_\lambda$ and if $\lambda < \lambda_0$, then $\rho(S_\lambda(t)) \to 0$, $\frac{d}{dt}\rho(S_\lambda(t)) < 0$. Using the fact we have continuous initial data, we hope that for $\lambda = \lambda_0$, $\frac{d}{dt}\rho(S_{\lambda_0}(t)) \to 0$ as $t \to T_{\lambda_0}$ and $\rho(S_{\lambda_0}(t)) \to \rho_0$ for some finite constant $\rho_0 > 0$. Thus, our picture of U including trajectories should look like Figure 4. We computed these trajectories for a small number of initial surfaces $S_\lambda(0)$ for λ near λ_0. The results are given by the solid lines in Figure 5. Our goal then, is to locate the special trajectory $S_{\lambda_0}(t)$.

In general, we cannot a priori compute λ_0 exactly. Regardless of how small $|\lambda - \lambda_0| > 0$ is, $S_\lambda(t) \not\to S_{\lambda_0}(t)$ as $t \to T_\lambda$. Therefore, we must find some other means of locating the trajectory $S_{\lambda_0}(t)$. To do this, we first define $R(\lambda, t) = \rho(S_\lambda(t))$. For $\lambda < \lambda_0$, $R(\lambda, t) \to 0$, $\frac{\partial R}{\partial t}(\lambda, t) < 0$ as $t \to T_\lambda$. Similarly, for $\lambda > \lambda_0$, $R(\lambda, t) \to +\infty$, $\frac{\partial R}{\partial t}(\lambda, t) > 0$ as $t \to T_\lambda$. Also, if the curvature does not blow up too fast, then we may conclude $\frac{\partial R}{\partial t}(\lambda_0, t) \to 0$ as $t \to T_{\lambda_0}$. Thus, we define $\tilde{\lambda}_0(t)$ such that $\frac{\partial R}{\partial t}(\tilde{\lambda}_0(t), t) \equiv 0$. The dashed line in Figure 5 depicts the function $R(\tilde{\lambda}_0(t), t)$. Then the idea of the algorithm for finding a self-similar solution is to compute $\lim_{t \to T_{\lambda_0}} S_{\tilde{\lambda}_0(t)}(t)$.

We now give the details of the general method. Recall that the level set formulation for curvature flow can be expressed as

$$\phi_t = \kappa_\phi ||\nabla \phi||. \tag{1}$$

We define a new function ψ as

$$\psi(x, t) = \phi(\sigma(t)x, t)/\sigma^2(t) - L(t). \tag{2}$$

Differentiating Equation 2 with respect to t and combining with Equation 1

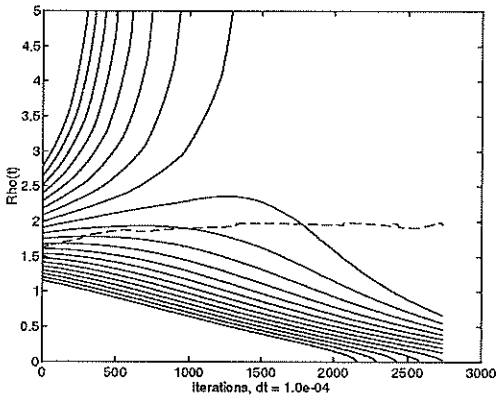

Figure 5: Computed trajectories of $S_\lambda(t)$

produces a new partial differential equation for ψ given by

$$\psi_t = \frac{\sigma'(t)}{\sigma(t)}(x \cdot \nabla\psi - 2(\psi + L(t)) + \kappa_\psi ||\nabla\psi|| - L'(t). \tag{3}$$

Here κ_ψ is the mean curvature of the level set surface of ψ through the point (x,t).

The functions $\sigma(t)$ and $L(t)$ are determined dynamically as time evolves. The stretching function $\sigma(t)$ is chosen so that the zero level set of ψ has constant volume for all t. Let $V(t) = \text{Volume}(\psi(\cdot,t)^{-1}(0))$, then

$$\sigma(t) = \left(\frac{V(t)}{V(0)}\right)^{1/3}$$

so that

$$\frac{\sigma'(t)}{\sigma(t)} = \frac{V'(t)}{3V(t)}.$$

The level function $L(t)$ is given by the equation

$$\frac{\partial R}{\partial t}(L(t),t) = 0.$$

In this context, we have $S_{\tilde{\lambda}_0(t)}(t) = \psi^{-1}(\cdot,t)(0)$.

We compute $\psi(x,t)$ numerically in a three step explicit scheme. The three steps are summarized below where $\psi_n \equiv \psi(x_{ij},t_n)$, $\Delta t = t_{n+1} - t_n$.

1. $\tilde{\psi}_{n+1} = \psi_n + ||\nabla\psi_n||\kappa(\psi_n)\Delta t$.
2. (a) • $V_{n+1} = \text{Volume}(\tilde{\psi}_{n+1}^{-1}(0))$

(b)
- $V_n = \text{Volume}(\psi_n^{-1}(0))$
- $R_n(\ell) = \rho(\psi_n^{-1}(\ell))$
- $R_{n+1}(\ell) = \rho(\tilde{\psi}_{n+1}^{-1}(\ell))$
- $L_{n+1} = (R_{n+1}(\cdot) - R_n(\cdot))^{-1}(0)$

3. $\psi_{n+1} = \tilde{\psi}_{n+1} + \frac{V_{n+1}-V_n}{3V_n}(x \cdot \nabla\psi_n - 2(\psi_n + L_n)) - (L_{n+1} - L_n)$

The first step is identical to the standard explicit numerical implementation of Equation 1. This is where the curvature flow terms appear. The second step is where $\sigma(t)$ and $L(t)$ are determined according to information obtained from the curvature flow in the first step. The third step makes the corrections to ψ needed due to the stretching and level set shifting predicted by the second step. Note that combining the first and third steps results in a straightforward explicit discretization of Equation 3.

In all cases, central differencing was used for spatial derivatives except for the term $x \cdot \nabla\psi_n$ where upwind differencing was used,

$$\begin{aligned} x \cdot \nabla\psi_n &= \max(0,x)D_-^x\psi_n + + \max(0,y)D_-^y\psi_n + \max(0,z)D_-^z\psi_n \\ &\quad + \min(0,x)D_+^x\psi_n + \min(0,y)D_+^y\psi_n + \min(0,z)D_+^z\psi_n. \end{aligned}$$

This follows the discretization used in [11].

Recall that $\frac{\partial R}{\partial t}(\lambda_0, t) \to 0$ as $t \to T_{\lambda_0}$, however this is expected only in a neighborhood of T_{λ_0}. In practice, $\left|\lambda_0 - \frac{\partial R}{\partial t}(\cdot, 0)^{-1}(0)\right|$ can be large causing problems numerically for small t. For that reason, we make a preliminary estimate of λ_0 by $\tilde{\lambda}_0$ using a bisection method, then step 2(b) for updating $L(t)$ is changed to

2. (b) $\ell = (R_{n+1}(\cdot) - R_n(\cdot))^{-1}(0)$
If $|L_n - \ell| < \epsilon$ then $L_{n+1} = \ell$ else $L_{n+1} = \tilde{\lambda}_0$.

This amendment delays the traversing of level sets until t is in a neighborhood of T_{λ_0}. We can see why this is a necessary precaution for small t in Figure 5 where $R(\tilde{\lambda}_0(t), t)$ (the dashed line) is not near the best approximation to $R(\lambda_0, t)$ (the middle solid line) for small t.

3 Tests for Self-Similarity

In Figure 6, we compare the profiles of the exact solution of the self-similar torus solution as derived from [1] represented by the solid line with the computed solution using our algorithm represented by the circles. The graph shows we have good agreement between these two solutions. For the other cases where an exact solution is not known, we will use other tests for self-similarity. For each test we will use the error for the computed torus solution as a benchmark for other solutions.

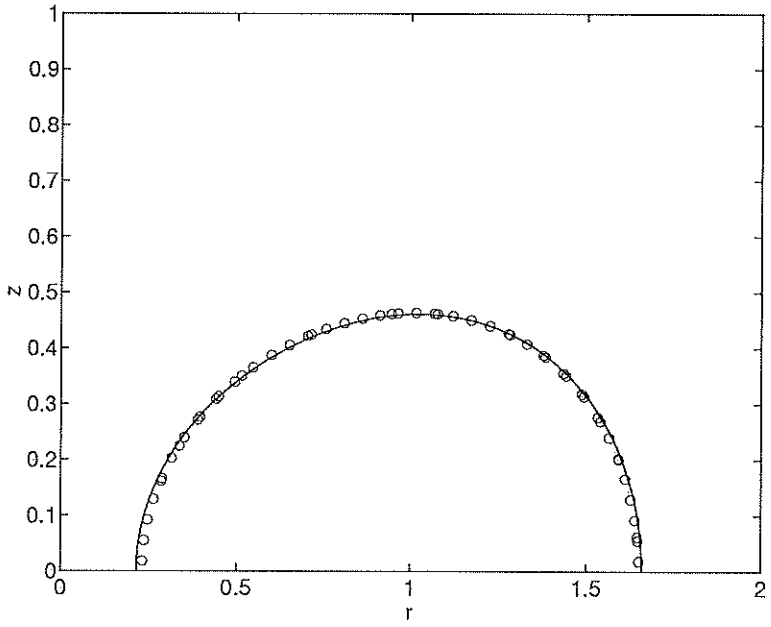

Figure 6: Comparison of computed and exact torus solutions

The first test of self-similarity is based upon the condition

$$\kappa - \frac{1}{2T} x \cdot n = 0$$

where κ is curvature, n is the unit normal, and T is the time to singularity. This is a necessary and sufficient condition for self-similarity. Given a surface S, we implement this test numerically by sampling evenly on S to get values x_i, n_i, and κ_i for $i = 1,\ldots,N$. The constant T is estimated by

$$T \approx \tilde{T} = \frac{\sum_{i=1}^{N} x_i \cdot n_i}{2 \sum_{i=1}^{N} \kappa_i}.$$

The computed error estimate is given by

$$E = \frac{1}{N} \sqrt{\sum_{i=1}^{N} \left(\kappa_i - \frac{1}{2\tilde{T}} x_i \cdot n_i \right)^2}.$$

For the computed torus on a rectangular grid of dimensions $90 \times 90 \times 90$ with space step size $\Delta x = 2.24 \times 10^{-2}$, the computed error is $E = 0.034354$. We conclude a surface is near self-similarity if E is of the same order as the computed error for the torus.

The second test is related to the first, but allows for differences in scale. If we plot the data points computed on a given surface with $\frac{1}{2\tilde{T}} x_i \cdot n_i$ versus κ_i, then the points should fill a diagonal line segment. We show the plot for the computed torus solution. Surfaces that fail this test tend to show some structure forming a significant angle to the expected line segment and do not decrease with time or grid refinement.

Finally, we start with the computed solution and evolve it according to normal mean curvature flow. A self-similar solution should retain its shape for a considerable time as it shrinks.

4 Computed Solutions

For each of the examples of computed solutions given below, we will describe the initial level sets and the measurements used for the ratio function $R(\lambda, t)$. We will follow that with pictures of the surface along with results from the tests discussed from the previous section and a brief summary.

We begin with a surface we call the "cube". The initial surface consisted of a sphere minus cylinders along the coordinate axes as depicted in Figure 8. The other level sets were equidistant contours from that initial surface. The ratio function measured the distance from the origin to the furthest point of the surface in the direction of the vector $(1, 1, 1)$ over the minimum radius of the hole along the x-axis as shown in Figure 9.

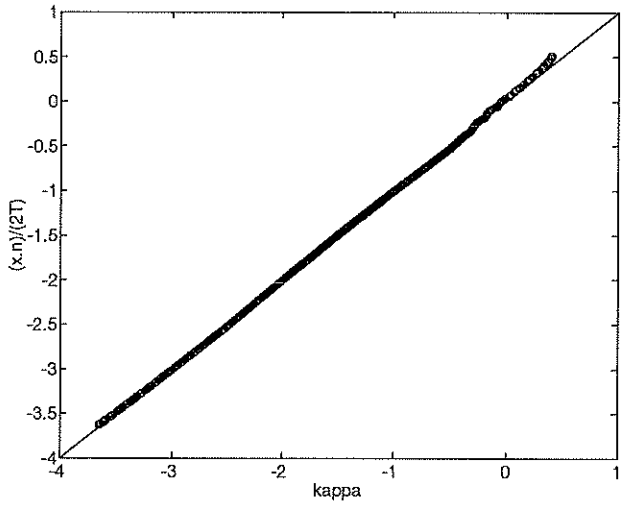

Figure 7: Graph of $\frac{1}{2T} x_i \cdot n_i$ versus κ_i for torus

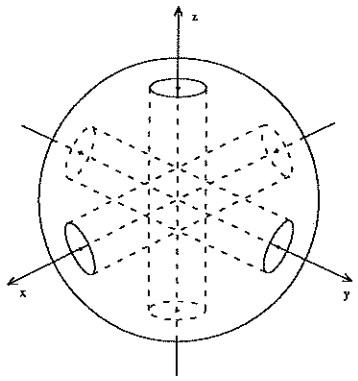

Figure 8: Initial surface for cube

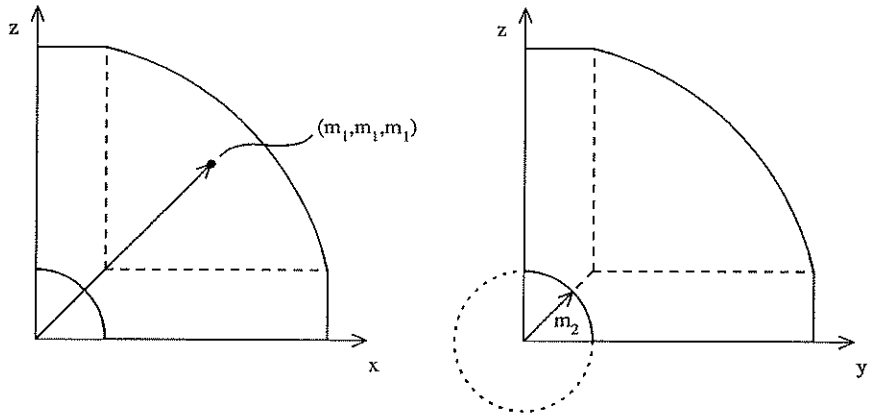

Figure 9: Ratio measurements for cube

The final computed solution is shown in Figure 10. The computation was performed on a $60 \times 60 \times 60$ grid with space step $\Delta x = 3.39 \times 10^{-2}$. The computed error for this surface is $E = 2.886 \times 10^{-2}$. The plot of $\frac{(x_i \cdot n_i)}{2T}$ versus κ_i is shown in Figure 11. This plot shows the characteristic lining up along the diagonal of the points on the surface. Finally, we show in Figure 12 one octant of this surface next to the same surface after it has evolved during normal mean curvature flow. Notice that it has retained its shape very well despite shrinking to almost 1/8 of its original volume.

The cube surface appears to pass all the tests for self-similarity within the guidelines of the computed torus solution, so we expect that this surface is a good approximation to a self-similar solution. This surface leads to the conjecture that every regular polyhedron with holes will produce a corresponding self-similar solution for mean curvature flow.

A natural next attempt for the algorithm would be to try other symmetric arrangements of holes through a sphere. For example, we started with an initial surface as described for the cube, except the hole along the z-axis is removed. Again, the other initial level sets are equidistant contours from this surface. We tried a few different ratio function measurements all with the same end results. One such pair of measurements consists of measuring the minimum width of the hole along the x-axis against the maximum width of one of the four holes made by the surface sliced by the xy-plane. We show these measurements in Figure 13

The final computed solution was underresolved in the center for every grid size we used. The best resolution produced the surface shown in Figure 14. The grid size for this surface is $60 \times 60 \times 120$ with space step $\Delta x = 3.39 \times 10^{-2}$. The computed error for this surface is $E = 5.14 \times 10^{-1}$ and the plot of $\frac{(x_i \cdot n_i)}{2T}$ versus κ_i is in Figure 15.

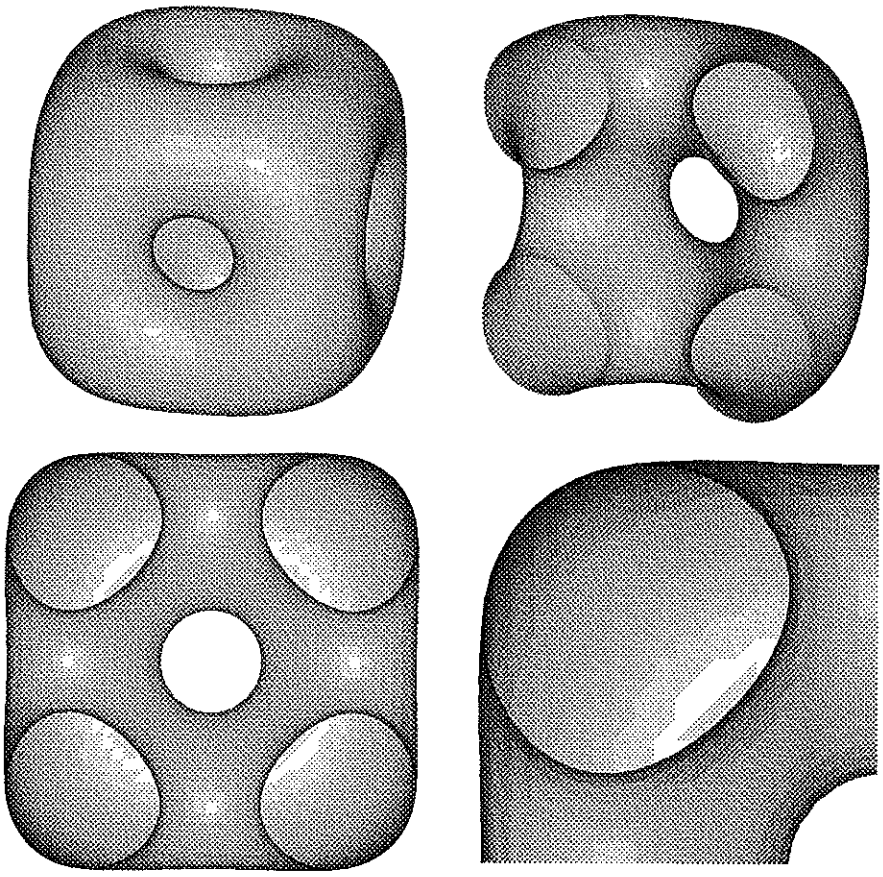

Figure 10: Pictures of the cube self-similar solution

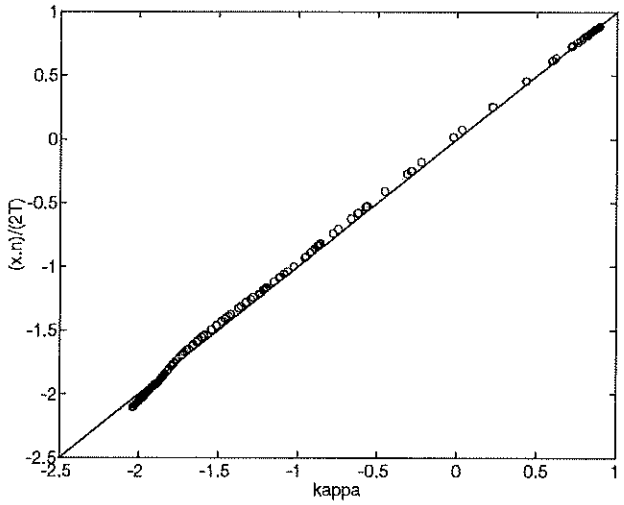

Figure 11: Graph of $\frac{1}{2T}x_i \cdot n_i$ versus κ_i for cube

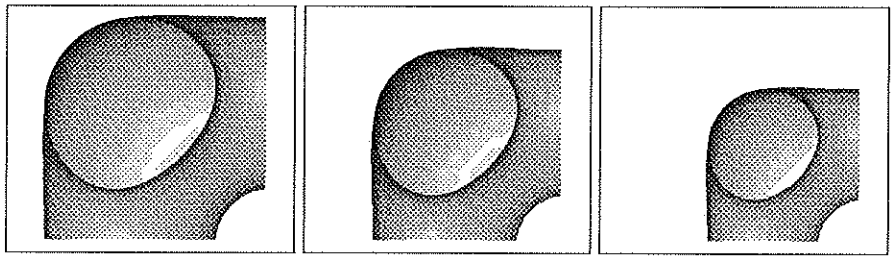

Figure 12: Cube surface evolved by mean curvature flow

Notice in Figure 15 the additional branch of points. This tail does not diminish with time as for other surfaces. The computed error is also much larger than acceptable to conclude this surface is self-similar. We believe that one of two things are true about this surface, either the size of the two spheres is so much larger than the central structure that we were unable to adequately resolve both or the true self-similar solution for this symmetric alignment is singular at the origin. The latter alternative is not appealing because it suggests that even with enough symmetry to fit into the framework of this algorithm, there is still no guarantee that $S_{\lambda_0}(T_{\lambda_0})$ exists. In either case, we are forced to conclude that this surface is not necessarily close to a self-similar solution.

In view of the this result, we return to the first conjecture and attempt to find a self-similar solution based upon a regular octahedron. Again we begin with

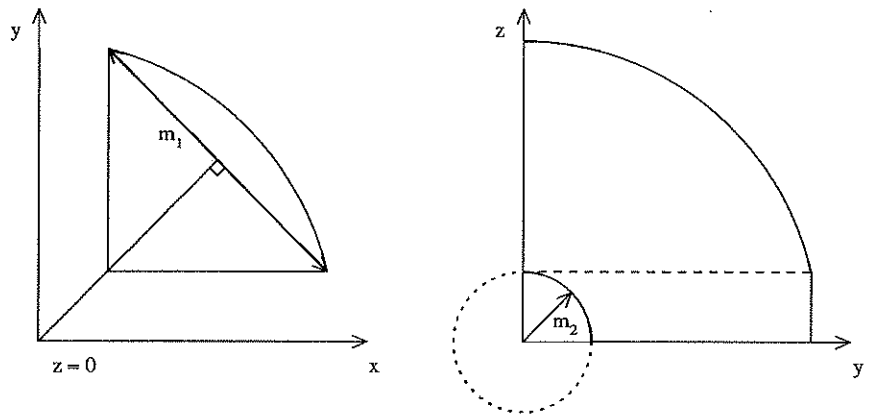

Figure 13: Ratio function measurements for the cube without one hole

a sphere, this time with holes drilled diagonally along the vectors $(\pm 1, \pm 1, \pm 1)$. The remainder of the construction follows almost identically to the construction for the cube.

The final solution for the octahedron is shown in Figure 16. The computation was on a $80 \times 80 \times 80$ grid with $\Delta x = 2.53 \times 10^{-2}$. The computed error for this surface is $E = 3.33 \times 10^{-2}$ and the error plot is shown in Figure 17. In Figure 18, we show the the initial solution and the result of evolving the surface.

For this surface, we get results which are sufficient to believe that the octahedron surface is a self-similar solution.

5 Conclusion and Future Work

We have presented here an algorithm which we believe is capable of computing self-similar solutions of mean curvature flow. In particular, we have computed self-similar surfaces which have been speculated to exist, but have not been verified theoretically. We hope that these solutions will aid in proving the existence (or non-existence) of new self-similar solutions.

One shortcoming of this approach is the symmetry restriction for solutions. We intend to remove one degree of freedom from this restriction by increasing the dimension of the space $S_\lambda(0)$ to two, and thus the space U will have dimension three. In this case, we will have two ratio functions ρ_1, ρ_2 for selecting trajectories within U. The resulting calculation should be possible within R^4, otherwise the computing expense will be too great.

In this higher dimension, we hope to find more self-similar solutions which are not currently possible with the current method. Two of our intended solutions

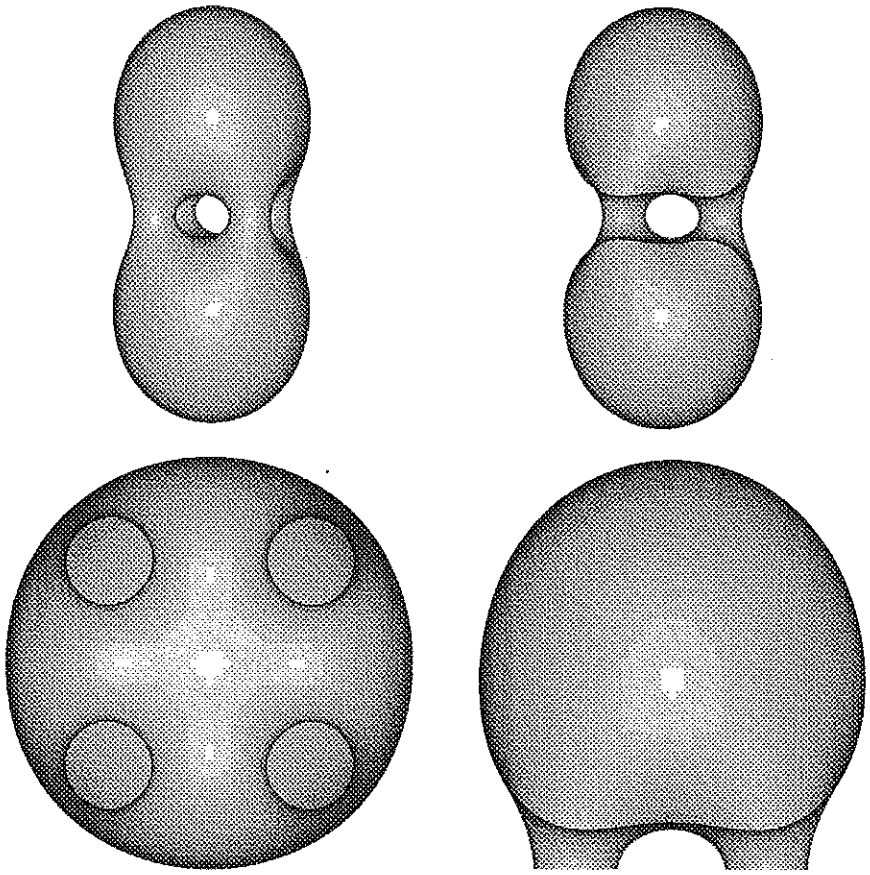

Figure 14: Computed solution for the cube minus one hole

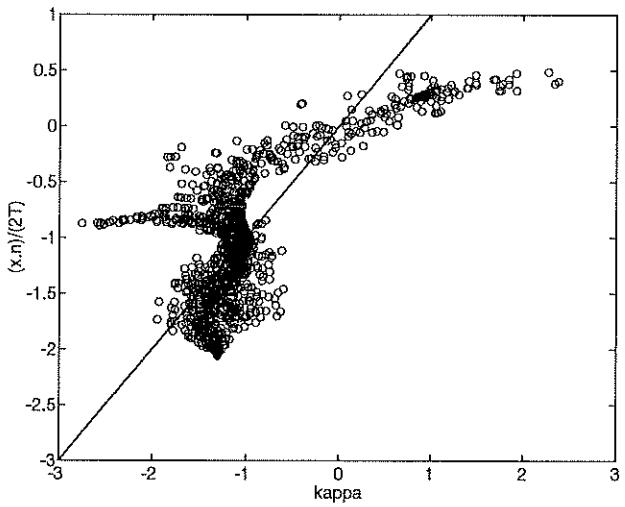

Figure 15: Graph of $\frac{1}{2T} x_i \cdot n_i$ versus κ_i for cube minus one hole

will be semi-regular polyhedra and a trefoil knot amongst others.

5.1 Acknowledgment

We would like to thank L. Craig Evans, Tom Ilmanen, Doug Jungreis, Sigurd Angenent, Gerhard Huisken, James Sethian, Peter Smereka, and Stan Osher for helpful comments and suggestions. This work is supported in part by a National Science Foundation Postdoctoral Fellowship.

References

[1] S. Angenent. Shrinking doughnuts. In *Nonlinear Diffusion Equations and Their Equilibrium Stats, 3*, 1992.

[2] Y. Chen, Y. Giga, and S. Goto. Uniqueness and existence of viscosity solutions of generalized mean curvature flow equations. *Journal of Differential Geometry*, 33:749–786, 1991.

[3] L. C. Evans and J. Spruck. Motion of level sets by mean curvature I. *Journal of Differential Geometry*, 33:635–681, 1991.

[4] L. C. Evans and J. Spruck. Motion of level sets by mean curvature II. *Transactions of the American Mathematical Society*, 330:321–332, 1992.

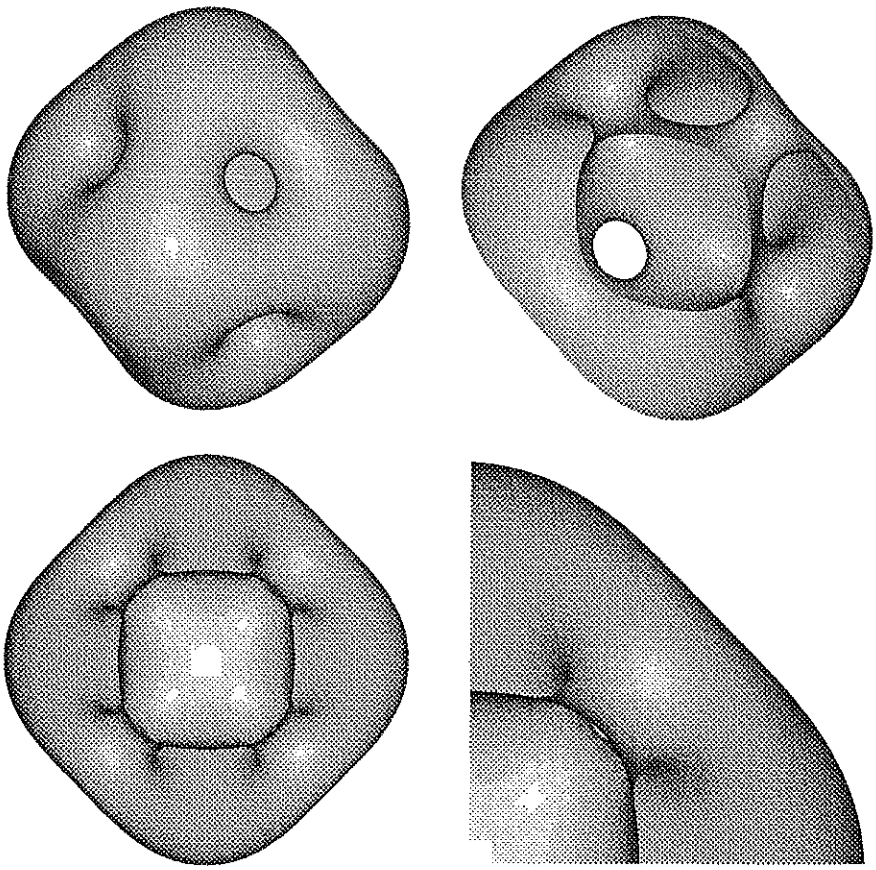

Figure 16: Self-similar octahedron surface

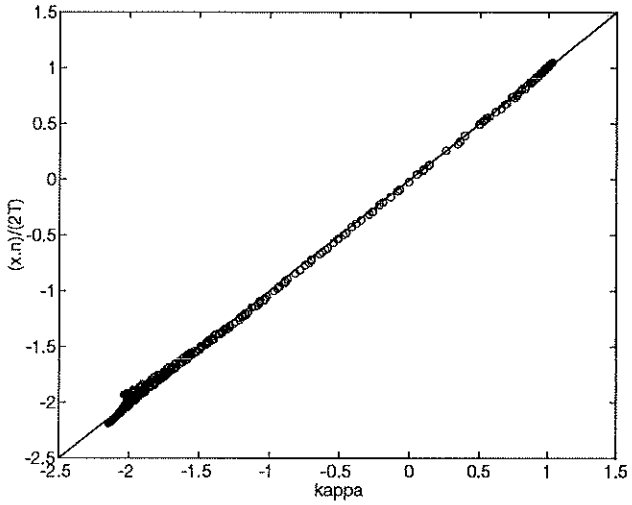

Figure 17: Graph of $\frac{1}{2T}x_i \cdot n_i$ versus κ_i for octahedron

[5] M. Falcone, T. Giorgi, and P. Loretti. Level sets of viscosity solutions and applications. Technical report, Instituto per le Applicazioni del Calcolo, Rome, 1990. preprint.

[6] Y. Giga and S. Goto. Motion of hypersurfaces and geometric equations. *Journal of the Mathematical Society of Japan*, 44(1):99–111, 1992.

[7] M. Grayson. The heat equation shrinks embedded plane curves to round points. *Journal of Differential Geometry*, 26(285), 1987.

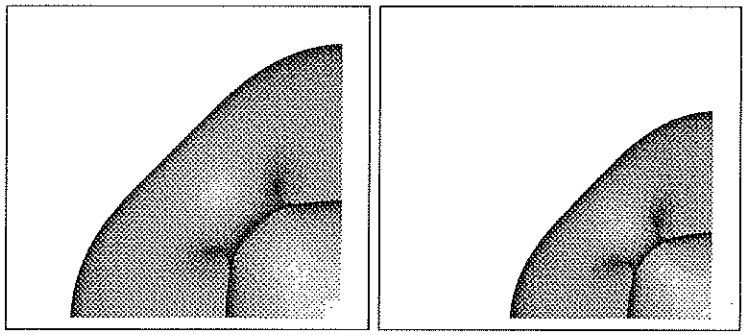

Figure 18: Octahedron evolved by mean curvature flow

[8] M. Grayson. A short note on the evolution of surfaces via mean curvature. *Duke Mathematical Journal*, 58:555–558, 1989.

[9] G. Huisken. Flow by mean curvature of convex surfaces into spheres. *Journal of Differential Geometry*, 20:237–266, 1984.

[10] G. Huisken. Asymptotic behavior for singularities of the mean curvature flow. *Journal of Differential Geometry*, 31, 1991.

[11] S. Osher and J. A. Sethian. Fronts propagating with curvature-dependent speed: Algorithms based on Hamilton-Jacobi formulations. *Journal of Computational Physics*, 79(1), November 1988.